Observation of centimetre-scale argon diffusion in alkali feldspars: implications for $^{40}Ar/^{39}Ar$ thermochronology

STEPHANIE FLUDE[1,2]*, ALISON M. HALTON[1], SIMON P. KELLEY[1], SARAH C. SHERLOCK[1], JAMES SCHWANETHAL[1,3] & CAMILLA M. WILKINSON[1,4]

[1]*Department of Earth and Environmental Sciences, The Open University, CEPSAR, Walton Hall, Milton Keynes MK7 6AA, UK*

[2]*Present address: QUADLAB, ENSPAC 12.1, Roskilde University, 4000 Roskilde, Denmark*

[3]*Present address: London Geochronology Centre, Department of Earth Sciences, University College London, Gower Street, London WC1E 6BT, UK*

[4]*Present address: Geological Survey of Norway, P. O. Box 6315, Sluppen, NO-7491, Trondheim, Norway*

**Corresponding author (e-mail: sflude@gmail.com)*

Abstract: New data from a gem-quality feldspar from Itrongay, Madagascar, record naturally occurring $^{40}Ar/^{39}Ar$ age profiles which can be numerically modelled by invoking a single diffusion mechanism and show that microtexturally simple crystals are capable of recording complex thermal histories. We present the longest directly measured, naturally produced $^{40}Ar^*$-closure profiles from a single, homogeneous orthoclase feldspar. These data appear to confirm the assumption that laboratory derived diffusion parameters are valid in nature and over geological timescales. Diffusion domains are defined by crystal faces and ancient cracks, thus in gem-quality feldspars the diffusion domain size equates to the physical grain size. The data also illustrate the potential of large, gem-quality feldspars to record detailed thermal histories over tens of millions of years and such samples should be considered for future studies on the slow cooling of continental crust.

Supplementary material: Ar-isotope data, standards and constants used in calculations and irradiation parameters are available at http://www.geolsoc.org.uk/SUP18720

Understanding the diffusive transport of argon in minerals, both within nature and the laboratory, is critical to our ability to apply $^{40}Ar/^{39}Ar$ data to thermochronological studies. Advances in laser spot and depth profile extraction techniques, and in stepped and cycle heating, have largely confirmed the Arrhenius relationship between diffusion rates and temperature (e.g. Foland 1974; Arnaud & Kelley 1997; Lovera *et al.* 1997; Wartho *et al.* 1999; Lovera *et al.* 2002), although recent analyses of argon diffusion at submicron spatial resolution (Watson & Cherniak 2003; Thomas *et al.* 2008; Baxter 2010; Clay *et al.* 2010) appear to indicate more than one diffusion mechanism in silicates. In contrast to the general consensus over the relationship between diffusion rates and temperature, there has been considerable debate and uncertainty concerning argon-loss systematics resulting from complexity in sample microstructure, including perthite boundaries, subgrains, and fast diffusion pathways. It has been hypothesized that multipath diffusion combining lattice diffusion and diffusion via defect pathways might act to limit the effective domain size to less than the visible grains (e.g. Lee 1995).

Parsons *et al.* (1988) and Burgess *et al.* (1992) demonstrated that alkali feldspar 'patch' perthite domain boundaries define diffusion domains while 'tweed' perthite domain boundaries do not. Further, Reddy *et al.* (2001) showed that apparent ages within a detrital K-feldspar did not vary across coarse perthite boundaries, indicating that such boundaries do not always act as diffusion domain boundaries, but in the same sample deformation-induced microstructures did define diffusion domains. More recently, Mark *et al.* (2008) showed that the smallest observed subgrains do not always define diffusion domains in authigenic K-feldspar. In summary, there have been several datasets on natural argon diffusion in complex samples but not in individual K-feldspar domains. We note that the debate continues in articles in the present special

From: JOURDAN, F., MARK, D. F. & VERATI, C. (eds) 2014. *Advances in $^{40}Ar/^{39}Ar$ Dating: from Archaeology to Planetary Sciences*. Geological Society, London, Special Publications, **378**, 265–275.
First published online January 10, 2013, http://dx.doi.org/10.1144/SP378.25

issue. Our motivation in analysing large individual grains of gem-quality K-feldspar was to test the coherence of argon diffusion in large grains from the micron scale at the grain surface to bulk diffusion over many millimetres within the same grain.

The Itrongay feldspar from Madagascar is an ideal sample on which to test the coherence of diffusion and the potential for multiple diffusion mechanisms for argon in K-feldspar. It is a clear, yellow-coloured, pegmatitic low-sanidine/orthoclase feldspar and detailed descriptions of various samples have been previously published (Coombs 1954; Wartho *et al.* 1999). Pegmatites generally form rapidly from supersaturated, undercooled fluids so are unlikely to be maintained at high temperatures for long periods of time (London 1996). Thus, the simple microtexture of Itrongay feldspar was thought to reflect a combination of both the simple geological history and the purity of the orthoclase (Or) composition lattice. Given the apparent simple crystal structure and rapid formation, these crystals represent an excellent natural laboratory to test the models for bulk argon diffusion which cannot be imaged in smaller crystals, and thus have to be inferred from low resolution laser profiles or from cycle or stepped heating experiments. Published radiometric ages for Itrongay feldspar range from 435 Ma (Arnaud & Kelley 1997) to 461 Ma (Wartho *et al.* 1999; Nägler & Villa 2000) using the $^{40}Ar/^{39}Ar$ dating technique, and up to 477 Ma for K/Ca ages (Nägler & Villa 2000). While the presence of this age discrepancy has been noted (Wartho *et al.* 1999) only Nägler & Villa (2000) have discussed possible causes; they have invoked either a discrete thermal disturbance or maintenance of temperatures above 350 °C as mechanisms that would have resulted in resetting of the $^{40}Ar/^{39}Ar$ system.

We have investigated two samples of Itrongay K-feldspar: one which was cut from a fragment of a larger grain (Crystal A, Fig. 1b); and a second sample which was a complete crystal exhibiting an untwinned euhedral shape and the characteristic monoclinic crystal habit (Crystal B, Fig. 1c). The perfect shape of Crystal B indicates that the crystal surfaces are original and formed as the pegmatite crystallized. Their origin and the planar form of these crystal surfaces make them ideal targets for the same depth profiling that has been used for the analysis of laboratory induced argon diffusion (e.g. Arnaud & Kelley 1997; Wartho *et al.* 1999).

Argon diffusion in Itrongay feldspar

Arnaud & Kelley (1997) investigated diffusion in the Itrongay feldspar by combined cycle heating, laser depth profiling and crushing on millimetre-sized fragments. Their data showed age variations related to domains that differed in size by a factor of around five, but the sizes were unspecified. The conclusions of combining laser depth profile measurements of ^{39}Ar appeared to indicate grains acting as single diffusion domains with some evidence for fast-path diffusion, an observation backed up by the better fits achieved in Multi-Domain Diffusion (MDD) modelling by the use of variable activation energies. In addition, sample crushing appeared to indicate traps in the structure with the potential to retain argon relative to the mineral lattice. Arnaud and Kelley concluded that volume diffusion took place over scales of at least 100 μm and that defects in the crystal acted as a reservoir for an apparent excess ^{40}Ar component. These traps were also considered to influence argon loss from the outer 10 μm of the sample and to act as fast diffusion pathways once they were opened to the surface during sample preparation. Subsequent UV laser depth profiling provided high spatial resolution analysis of laboratory induced argon diffusion. Samples were heated in a high pressure argon atmosphere by Wartho *et al.* (1999), who concluded that argon diffusion occurred by volume diffusion to the visible grain boundary. The diffusion parameters from these studies corroborated the accepted laboratory values of activation energy (E) and pre-exponential factor (D_0) for alkali feldspars and values determined by step heating and cycle heating of natural samples. While it has been implied that argon diffusion domains in Itrongay feldspar should equate to physical grain sizes, Arnaud & Kelley (1997) hypothesized fast-track diffusion in the outermost few microns, and other studies have measured varying laboratory diffusion and solubility in the outermost micron (Watson & Cherniak 2003; Thomas *et al.* 2008; Baxter 2010; Clay *et al.* 2010).

Sample preparation and $^{40}Ar/^{39}Ar$ methodology

Two samples of Itrongay alkali feldspar were used for this study: the first (Crystal A) was a 100 μm thick polished slice (final polish using 0.3 μm aluminium oxide paste) cut from a larger broken crystal more than 1 cm in diameter (Fig 1b); the second sample (Crystal B) was a whole crystal exhibiting a characteristic feldspar monoclinic shape and thus ancient crystal boundaries (Fig. 1c). From Crystal B we sampled three crystal surfaces to a depth of *c.* 1 mm using a slow saw (Fig. 1d). We were able to sample the [010], [110] and [101] crystal faces to test for varying argon diffusion rates. We noted that the [010] and [101] faces

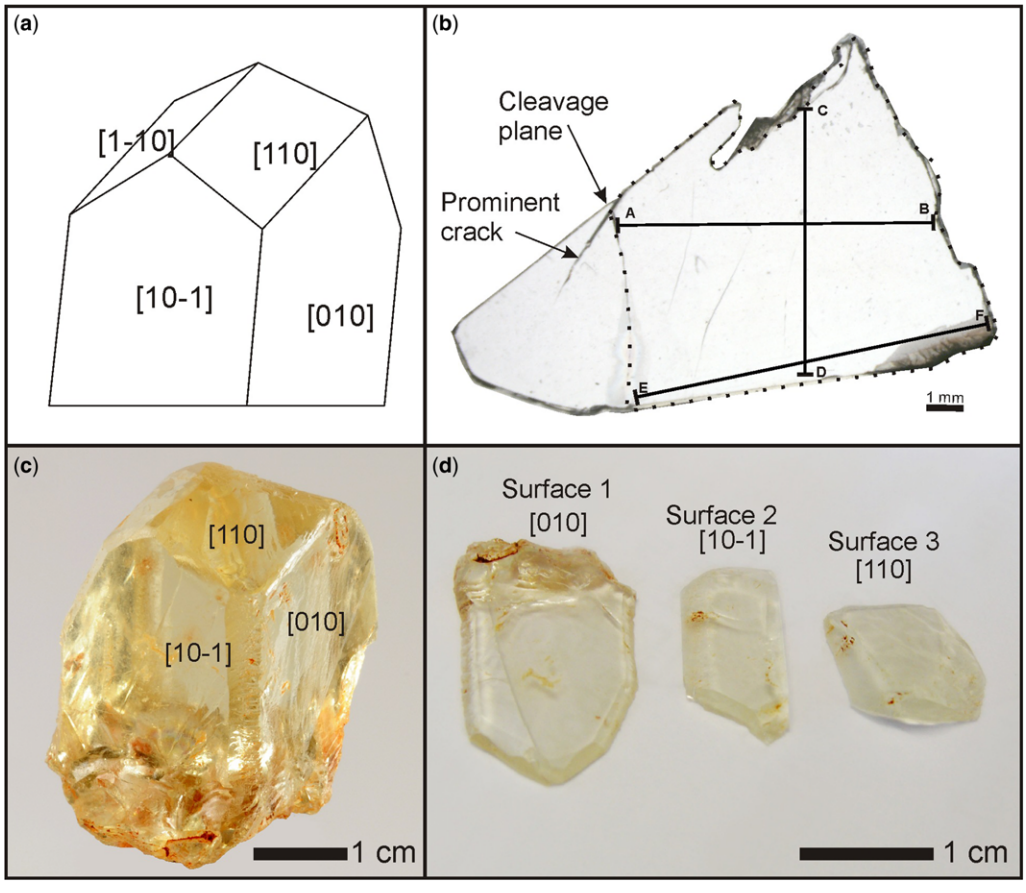

Fig. 1. (**a**) Cartoon of a perfect orthoclase feldspar crystal showing the crystal habit and faces. (**b**) Image of the polished slab from Crystal A. The dotted line shows the fragment of this slab that was irradiated and analysed. Black line show the positions of the $^{40}Ar/^{39}Ar$ age profiles discussed in the text. This crystal is an offcut from a larger crystal and no original crystal faces are visible. (**c**) Photograph of Crystal B. (**d**) Photograph of the surfaces sampled via slow saw from Crystal B.

were very near planar (although scratched) and we interpret these as representing the original crystal faces, while the [110] sample was considerably more undulating, possibly representing loss of material from the surface. Selected slices of the two samples were ultrasonically washed in acetone and distilled water, dried, wrapped in aluminium foil and irradiated at the McMaster Reactor (Canada) using cadmium shielding. The neutron flux was monitored using biotite standard GA1550, which has an age of 99.8 ± 0.2 Ma (Renne *et al.* 1998, 2010) and gave J-values of 0.01041 ± 0.000052 and 0.01265 ± 0.000063. Standards were analysed by melting *in vacuo* using an infrared 1090 nm fibre laser to melt individual biotite grains. Gases were cleaned by getters in a similar manner to the Itrongay samples, except that an in-line cold finger was used to reduce water and carbon dioxide prior to gettering. The cleaned gases from the standards were analysed using an MAP 215–50 noble gas mass spectrometer.

A New Wave Research Ltd LUP 213 nm pulsed quintrupled Nd-YAG laser was used to ablate the K-feldspar samples producing two different types of profiles. Pits *c.*100 μm in diameter were ablated producing a traverse across the polished and cleaved surfaces, and depth profiles from the natural crystal surfaces were produced by repeated rastering over 200 μm squares (see Wartho *et al.* 1999). Three transect profiles were analysed on the polished surface of Crystal A, creating age profiles nearly 1 cm long. Each of the three ancient surfaces of Crystal B was analysed twice, creating six depth profiles of around 20 μm. In addition, since the laser ablation process is inefficient at great depths, we cleaved two of the three ancient crystal

surfaces to reveal fresh surfaces orthogonal to the crystal face and created ablation traverses up to 1 mm depth into the original crystal using laser spots. Once the gas released had equilibrated in the extraction system, two SAES getters removed unwanted gas species over a period of less than 5 min, one operating at room temperature and the other at 450 °C, for a minimum of 30 s prior to automatic inlet into the Nu Instruments Noblesse noble gas mass spectrometer. Interfering hydrocarbon and chlorine peaks were measured at masses 35, 36 and 39 in addition to the argon isotopes to monitor for hydrocarbon or chlorine interferences, none of which were observed at levels greater than system blanks. Hydrocarbon peaks at masses 36 and 39 were measured as shoulders on the side of the argon peaks, always at the high mass side. All analyses were corrected for blanks,^{37}Ar decay and neutron-induced ^{40}Ar (using the correction factor $(^{40}Ar/^{39}Ar)_K = 0.0085$); Ca-derived ^{39}Ar and ^{36}Ar were not corrected for due to the very low abundance of Ca in Itrongay feldspar (10 ppm: Nägler & Villa 2000) resulting in measured levels of $^{37}Ar_{Ca}$ being indistinguishable from the blank. Yields of ^{36}Ar were low in all analyses, although it was always measurable in the analysis of the natural crystal surfaces. In many analyses, however, ^{36}Ar measurements were indistinguishable from the blank even when averaged over a day. Regular monitoring of the ^{36}Ar peak position, instrument background and hydrocarbon peaks confirmed that the low ^{36}Ar yields are genuine and not due to measurement error or reduced detection limits from an elevated instrument background. In addition, detailed analysis of both young sanidines and mineral standards, using a similar approach to Renne *et al.* (2012) on the same instrument, confirmed that this procedure ensures the correct measurement of ^{36}Ar. Therefore, these low ^{36}Ar yields are considered to reflect very low ^{36}Ar levels within the sample. Where the ^{36}Ar yields are indistinguishable from or lower than the blank (i.e. the blank-corrected ^{36}Ar value is zero or negative), it is assumed that the atmospheric argon content of the analysis is effectively zero.

Results

Crystal A argon-isotope and age data are given in the supplementary data table S1 and the ages are shown in Figure 2. The ages range from 450.3 ± 2.4 Ma to 473.8 ± 2.3 Ma, showing over 20 Ma of age variation. Most of this age range is included in an 8 mm long profile (A–B) across the slab (Fig. 2). This profile shows a steep increase in age from *c.* 450–458 Ma within the first millimetre, followed by a gentler increase to *c.* 469 Ma at 4 mm where the profile plateaus. This profile begins within the crystal, at the edge of a fragment of the polished slab, the edge being formed by a cleavage plane next to a pre-existing crack in the crystal (Fig. 1b).

Profile C–D, which runs orthogonal to the other profiles, shows a smooth but less pronounced increase in age (*c.* 464 to *c.* 473 Ma) from the top to the bottom of the slab. The final profile (E–F) runs horizontally across the bottom of the slab and shows a slight, but insignificant age increase from left (471 Ma) to right (473 Ma). As a whole, the slab shows an increase in age from the top left corner to the bottom right.

The $^{40}Ar/^{39}Ar$ isotope and age data for Crystal B are given in the supplementary data table S2 and shown in Figure 3. Age variations are greater than for Crystal A, from as low as 415.7 ± 3 Ma to 471.2 ± 3.4 Ma, a range of 55 Ma (cf. 20 Ma range in Crystal A). Note, however, that the range only extends to lower values; the highest value for both crystals are within experimental errors and also agree closely with the determined K/Ca age for samples from the same locality (477 ± 2 Ma: Nägler & Villa 2000). When all age analyses of Crystal B are plotted against the distance from the crystal boundary (Fig. 3) they display a very coherent trend from young ages at the surface, increasing rapidly with distance at first to around 440 Ma by 20 μm depth, but rising at a decreasing rate at greater distances to reach around 470 Ma at 1 mm distance from the ancient crystal surface.

There is one departure from this pattern – the data we obtained from the third surface [110], which we noted was less regular in form than the two planar surfaces (see supplementary data table S2). Individual $^{40}Ar/^{39}Ar$ ages in this depth profile did not show any consistent variation with depth, and appeared to correspond with the highest ages in the other depth profiles. Ages ranged from 457.5 ± 3.6 Ma to 471.7 ± 3.1 Ma. It seems likely that the present surface was not a grain boundary during the time at which the other boundaries lost radiogenic argon. Given its more pitted appearance it seems likely that dissolution has taken place, and, since ages from other surfaces were consistently around 415–425 Ma, that up to several hundred microns have been lost from the surface. This observation also raises the possibility that mass has been lost at other crystal faces and that ages younger than 415–425 Ma may have been recorded (and subsequently lost) on completely undisturbed surfaces, but the planar nature of the [010] and [101] surfaces suggests that this is unlikely. We also cannot rule out the possibility that this is the original crystal surface, but it did not act as a boundary connected to an infinite reservoir – that is, it was not a grain boundary for diffusional argon loss. Mark *et al.* (2008) have shown that such effects can occur on

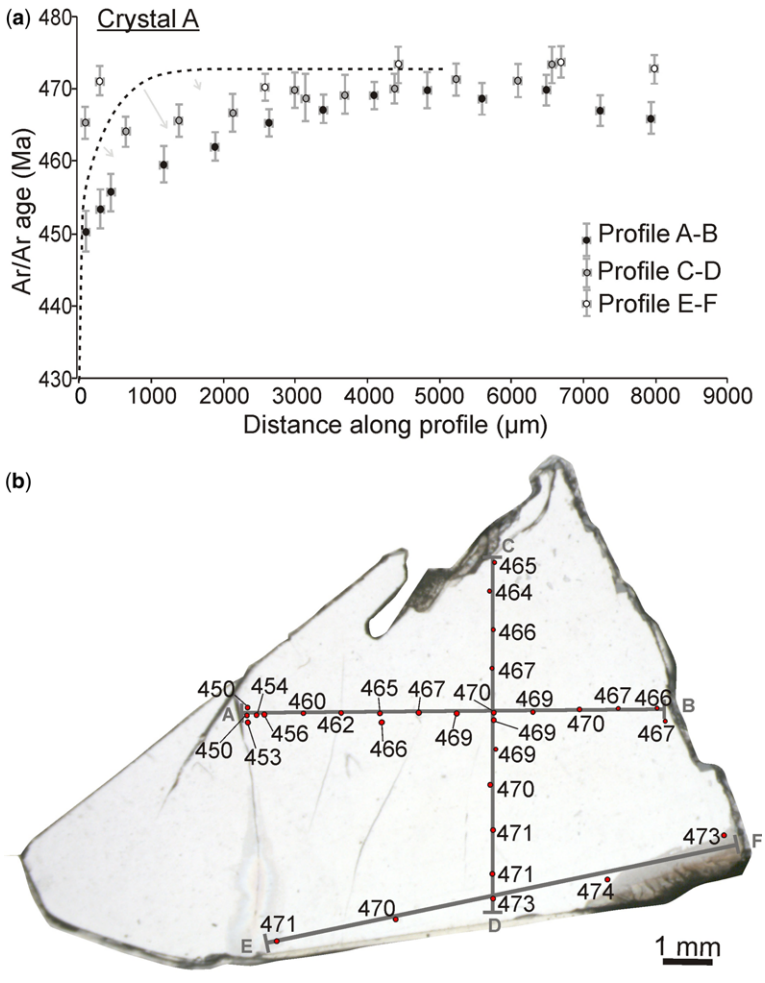

Fig. 2. Age profiles for Crystal A. Error bars are 2σ. The relative positions of the analyses and their ages are shown on the photomicrograph (cf. Fig. 1b) where ages are displayed rounded to the nearest Ma; errors are not shown but are $\pm 2-3$ Ma at 2σ. Dashed line represents the DIFFARG model of Scenario 3 (see text) and the arrows show the direction this curve is expected to move if an age profile was measured at an angle not perpendicular to the grain edge.

a micron scale in feldspar overgrowths, and there is evidence that mica grain boundaries have variable permeability (Smith *et al.* 2005) leading to variations in edge ages across one grain.

One feature of the Crystal B age profiles is that there is little variation between ages in different profiles at the same distance from the grain boundary. The only zone which deviates from this pattern is that of the outermost 2 μm where we recorded ages varying by over 10 Ma. However, we hesitate to place too much of our interpretation on this outer zone since we note that the crystal is visibly scratched on the two flat surfaces. Such variations from a perfect surface may lead to enhanced argon loss via fast-track diffusion pathways (i.e. loss via deformed lattice beneath the scratches), thus it may not be appropriate to interpret these ages in terms of volume diffusion and we place less emphasis on the outermost points while noting that the thermal history recorded lasted beyond the *c.* 425 Ma ages recorded by many points close to the grain edge. We also note that it is possible that the age profiles continue to steepen towards the grain boundary up to the final few nanometres such that we were unable to measure them, and that there is a pattern reflecting a younger thermal history in the outermost micron of the grain.

The coherence of all the profiles in the Crystal B data allows us to observe that the age profile appears to deviate from those that might be

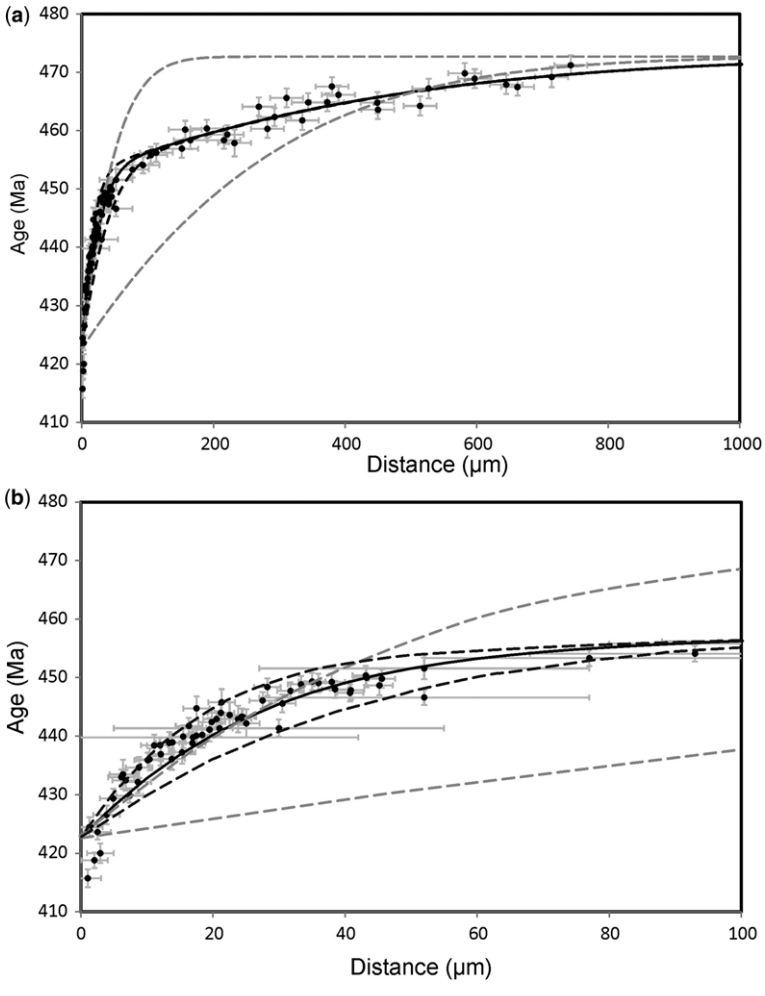

Fig. 3. Composite age profile from Crystal B showing data from depth profiles from the [010] and [110] crystal faces and deeper transects from all three surfaces (black circles with grey error bars representing 1σ). Dashed grey lines are DIFFARG modelled profiles using thermal history Scenario 1 (see text), reheating already cooled grains to 320 °C (lower line) and 270 °C (upper line) at 423 Ma. DIFFARG age profiles modelled using the two-stage thermal history of Scenario 3 (see text), which initially holds the grain at 350 °C, followed by cooling to 250 °C, 260 °C or 270 °C, are represented by solid (260 °C) and dashed (250 °C upper and 270 °C lower) black lines. (**a**) Full profiles to *c.* 1 mm depth. Profiles from all three crystal faces are remarkably coherent. (**b**) Age profiles showing the outermost 100 μm.

produced from rapid ^{40}Ar* loss or gain (e.g. Pickles *et al.* 1997) in that it appears to steepen close to the grain edge, resembling more closely a slow-cooling profile (Dodson 1986).

Argon diffusion modelling and discussion

All the age profiles described and illustrated in Figures 2 and 3 resemble age profiles resulting from diffusional loss of ^{40}Ar* across the whole crystal and thus centimetre-scale distances. Indeed to our knowledge these are the longest natural diffusion profiles yet recorded and are around an order of magnitude longer than previously known examples (e.g. Reddy *et al.* 2001). The implication of such long and coherent age profiles in a gem-quality alkali feldspar is that the thermal history reflects either long slow cooling, or reheating and loss of radiogenic argon at some point after the initial cooling. Pegmatites form rapidly from supersaturated undercooled liquids (e.g. London 1996), so the presence of these age profiles must represent

diffusional loss of $^{40}Ar^*$ through the crystal lattice during a prolonged thermal history. Since the thermal history of the region is already constrained (see below) we will be able to compare diffusion profiles produced by combined loss and radiogenic build up, as observed from natural diffusion, with models based on laboratory determined diffusion rates with natural diffusion.

Measurements at high spatial resolution of $^{40}Ar/^{39}Ar$ age profiles can be modelled, using the numerical model DIFFARG (Wheeler 1996), to reconstruct possible thermochronological histories for the sample. Conversely, where the thermal model is already known to some extent, such models can be used to test the assumptions underlying the model including the diffusion parameters E and D_0, the boundaries and grain size assumed, and also the relationship between diffusion rates measured in a laboratory and those extant in natural samples cooled on geological timescales. DIFFARG calculates radial age profiles that are perpendicular to the grain boundary. Comparison of modelled age profiles with our data provides insights into both the thermal history and diffusion of argon within the sample.

While it is not possible for modelled age profiles to be precisely fitted to the data for Crystal A because the crystal orientation and the precise location of original crystal surfaces are unknown, the measured age profiles suggest coherent diffusive loss of $^{40}Ar^*$ over distances of at least 1 cm. Fitting the precise shape using spherical or even one dimensional diffusion is open to some interpretation since we do not know the orientation relative to the ancient grain boundaries. However, we note that the minimum and maximum ages are comparable to the profiles from Crystal B, and while the youngest ages in Crystal A occur within the crystal, rather than at its edge, they are found close to two prominent cracks, one of which forms the edge of the fragment and is likely to be a cleavage plane. The most likely explanation of this age distribution is that the crystal acted as a single domain bounded by crystal edges and some early fractures, which resulted in diffusional $^{40}Ar^*$ loss both at the edges and along a plane which formed early in the thermal history. We also note that a non-perpendicular profile taken across a crystal displaying a concentric age distribution consistent with the profiles derived from Crystal B would produce an age profile with a reduced inflection and smoother change in gradient, similar to the profile derived from Crystal A. This means that the data from Crystal A are not necessarily inconsistent with the data from Crystal B, but precise modelling of the profile of Crystal A is not feasible due to uncertainties regarding the size of the crystal and the 3D orientation of its surfaces and cracks in relation to the age profile.

In contrast to Crystal A, the orientation and relationship (perpendicular) of the measured age profile to the crystal boundary is well characterized for Crystal B, and thus we have been able to directly compare measured and modelled age profiles to extrapolate considerably more detail of the thermal history of the area based on the known thermal history constraints and the argon-loss model which assumes the use of laboratory determined diffusion parameters (Wartho *et al.* 1999). The thermal history of Madagascar has been extensively studied in the context of the amalgamation and subsequent break-up of Gondwana, and thermochronological modelling of the $^{40}Ar/^{39}Ar$ data is likely to reflect these events. The Pan-African Orogeny began 650–700 Ma, with the later stages of continental collision occurring *c.* 550–570 Ma and final suturing completed by *c.* 535 Ma, with localized thermal perturbations relating to shear zones (Paquette & Nédélec 1998; Emmel *et al.* 2006; Grégoire *et al.* 2009; and references therein). Despite the localized thermal and structural complexities, various thermochronological studies from different terrains show similar cooling histories after *c.* 535 Ma (Fig. 4). We have used these models to provide constraints on the post-amalgamation cooling history of Madagascar for the area around Itrongay from where the feldspars derive. The final event occurred around 88 Ma when widespread magmatism and volcanism occurred in southern Madagascar over a 6 myr period, related to the Marion Hotspot and the separation of Madagascar from India (Storey *et al.* 1995). This may have caused crustal heating in southern Madagascar, although this was not identified by Seward *et al.* (2004).

We have assumed the thermal history started at 477 Ma based on the K/Ca age of Nägler & Villa (2000). The oldest ages recorded in either Crystal A or B are around 471 Ma in the core of the grains, and thus K-feldspar began to retain argon quantitatively *c.* 6 million years after the initial intrusion. Nägler & Villa (2000) suggested two thermal history scenarios to account for the difference between K/Ca and $^{40}Ar/^{39}Ar$ ages, based on the different diffusivities of calcium and argon, and on the monoclinic structure of the feldspar. However, both scenarios were based on the assumption that the oldest $^{40}Ar/^{39}Ar$ age is 461 Ma (previously measured on bulk samples), whereas our experiments have demonstrated that the oldest ages recorded are *c.* 471 Ma. In order to further constrain the thermal history and model the argon loss, we determined the youngest ages in the thermal history based on ages at the edge of Crystal B profiles, ignoring the youngest ages which appear

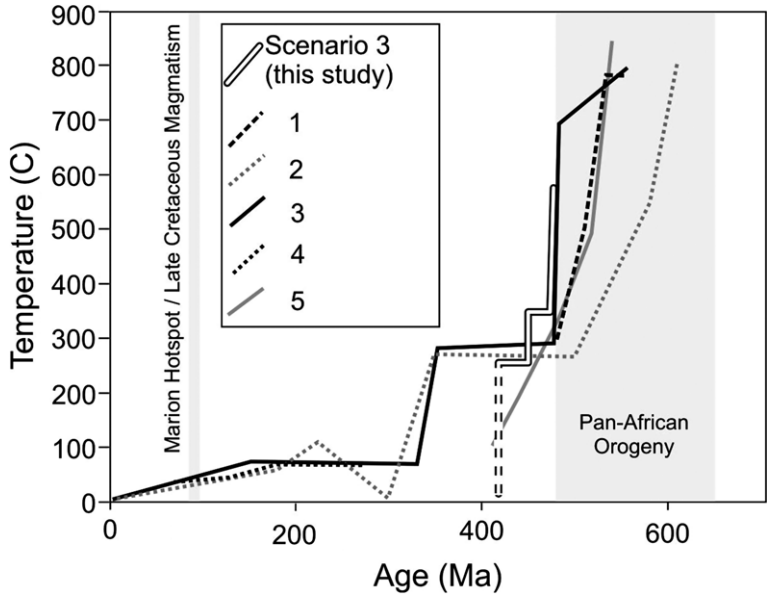

Fig. 4. Comparison of published thermal histories for central and southern Madagascar with the thermal history derived by DIFFARG modelling of age profiles from Crystal B. Published thermal histories are from: (1) Grégoire *et al.* (2009), based on monazite dating and amphibole and biotite $^{40}Ar/^{39}Ar$ ages; (2) Emmel *et al.* (2008), based on apatite and titanite fission track ages, biotite $^{40}Ar/^{39}Ar$ ages and titanite, zircon and monazite U–Pb, Pb–Pb and U–Th–Pb ages; (3) Emmel *et al.* (2006), based on titanite and apatite fission track dating; (4) Seward *et al.* (2004), based on zircon and apatite fission track ages and (5) Meert *et al.* (2001), based on U–Pb zircon ages and $^{40}Ar/^{39}Ar$ hornblende, biotite and K-feldspar ages. While the published thermal histories are quite variable, owing to their regional distribution over hundreds of kilometres and their varying tectonic origins (basement rocks, upper crustal rocks, metamorphism, plutonism), they nevertheless record a general cooling trend, which is consistent with our modelled thermal history.

to steepen suddenly in the outer 2 μm. We thus assume a youngest age of 423 Ma since it produces the best fits to the lower age data.

Three thermal history scenarios were modelled. In the first (Scenario 1) we attempted to model the age profiles based on a simple thermal history of pegmatite emplacement followed by rapid cooling to 471 Ma and subsequent reheating at 423 Ma to test whether this scenario reproduced the form of the age profiles in Crystal B. The two grey dashed lines in Figure 3 illustrate model curves for the scenario of reheating at 423 Ma for 1 myr to temperatures of 320 °C and 270 °C. The lower temperature produced an age profile that fits the ages in the outer 20 μm but not the rest of the profile. The higher temperature model fits the data between 400–800 μm from the crystal surface but not the data closer to the crystal surface. Thus neither these two end members nor any intermediate temperature reheating event produces a good fit to all the data and we conclude that the simple reheating model is not a valid explanation for the age profiles in Crystal B. We hypothesized above that the steepening of the profiles towards the grain boundary resembled slow cooling, but a linear cooling history (Scenario 2, various cooling rates modelled) produced a similarly poor fit because the age difference (50 myr) and difference in temperatures recorded are insufficient to produce the hypothetical 'Dodson slow cooling' patterns.

We noted that the thermal histories for Madagascar (Fig. 4) have a pattern that appears to indicate rapid initial cooling but then an extended history of much lower cooling rates, a process resembling 'cratonization' of the continental crust. Thus, in Scenario 3 (Fig. 4), we modelled a similar rapid cooling followed by a slower cooling pattern for the Itrongay sample. We used a simple two-step model to test this hypothesis although we note that this is not a unique solution. The model started with rapid cooling to 350 °C at the emplacent age of 471 Ma. This temperature was maintained for 20 myr and was followed by a second cooling to either 250 °C, 260 °C or 270 °C, which was maintained until 423 Ma (Fig. 4). This simple two-stage model produced an excellent fit to the data (Fig. 3). The best fit was for the model which combined 350 °C and 260 °C steps (solid line on Fig. 3); we

noted that all data points (other than the three points within 2 μm of the surface) fell within two sigma errors of the model curve and the majority less than one sigma from the curve. The two-step model reproduced the inflection in the age profile seen in Figure 3 and also conformed very closely to the known thermal history. This is not presented as a unique thermal history solution, but it does demonstrate that these crystals are capable of recording variations in thermal history and that a detailed thermal history could be recovered by more analytical work on a range of grains.

Our model thermal history for Itrongay (Fig. 4), which is based on a single diffusion pathway for K-feldspar, compares very well with the thermal histories for southern and central Madagascar derived from other sources, and potentially refines them since the lower bound on many of the histories is defined by either a single published apatite fission track age (Emmel *et al.* 2006) or an $^{40}Ar/^{39}Ar$ multi-domain modelled age-temperature pair for a K-feldspar in the Carion granite, north-central Madagascar (Meert *et al.* 2001). However, we note that it may also be possible to reproduce the observed profile with a simpler thermal history if two (or more) diffusion pathways for argon in K-feldspar are invoked (see Lee 1995; Baxter 2010), but we have not attempted to numerically model this due to a lack of model constraints. Nevertheless, an important conclusion is that the model thermal history, based on the age profiles in a single gem-quality alkali feldspar grain and laboratory diffusion parameters, reproduces the thermal history derived from other sources. This corroborates the assumption that laboratory derived diffusion parameters can be used to model natural diffusion over geological timescales. Furthermore, the coherency of the Crystal B age profiles confirms that argon diffusion in homogeneous K-feldspar is isotropic and does not occur at different rates depending on the crystallographic orientation.

Our analysis of a gem-quality grain appears to confirm the capability of the lattice to retain coherent argon closure profiles (a combination of diffusive loss and radiogenic build-up) over distances of many millimetres, confirming the capability of smaller subgrains or domains (that form above their closure temperature and remain unchanged) to retain genuine thermal histories in the form of closure profiles as hypothesized by the MDD model (Lovera *et al.* 1989, 1997, 2002). Conversely, laser profiles of the type illustrated above are only possible on the largest gem-quality grains, but there is considerable scope for similar studies in other areas that may be able to reveal slow cooling of continental crust.

Finally, we caution that, when using pegmatitic gem-quality feldspars for diffusion experiments, a simple geological and thermochronological history should not be assumed and that chemically homogeneous feldspars do not necessarily have a homogeneous distribution of argon isotopes; any simple argon-loss experiments should check the samples for pre-existing age gradients.

Conclusions

We conclude that the Itrongay alkali feldspar records closure age profiles formed over 50 million years, and thus natural argon diffusion in alkali feldspars can be explained by the same diffusion mechanism as that observed in short-term laboratory experiments. While we did detect an apparent variation from the trend in the outer 2 μm of the grain this is likely to be the result of surface imperfections and defects deviating from a planar surface behaviour in this sample. Our modelling, which used a thermal history consistent with published constraints, shows that this naturally occurring closure profile can be produced by invoking a single diffusion mechanism and that additional argon diffusion mechanisms, pathways or defect-enhanced fast-track diffusion are not necessarily required to reproduce the steepening in the outer few tens of microns of the age profile.

The thermal history and coherence of the closure profiles also explain variations in measured ages of different samples of Itrongay feldspar over the years, since the sampling location within the grain and the original grain size will have a profound effect upon the bulk age. Large gem-quality grains such as from the Itrongay sample have the capability to reveal long and slowly changing thermal histories for areas of continental crust such as Madagascar.

The authors gratefully acknowledge NERC grants NE/E018629/1 and NE/I016023/1. J. Wartho is thanked for providing the Itrongay feldspar sample. E. Baxter is thanked for a constructive review along with editors F. Jourdan and C. Verati.

References

ARNAUD, N. O. & KELLEY, S. P. 1997. Argon behaviour in gem-quality orthoclase from Madagascar: experiments and some consequences for $^{40}Ar/^{39}Ar$ geochronology. *Geochimica et Cosmochimica Acta*, **61**, 3227–3255.

BAXTER, E. F. 2010. Diffusion of noble gases in minerals. *Reviews in Mineralogy and Geochemistry*, **72**, 509–557.

BURGESS, R., KELLEY, S. P. *ET AL.* 1992. $^{40}Ar/^{39}Ar$ analysis of perthite microtextures and fluid inclusions in alkali feldspars from the Klokken syenite, South Greenland. *Earth and Planetary Science Letters*, **109**, 147–167.

Clay, P. L., Baxter, E. F., Cherniak, D. J., Kelley, S. P., Thomas, J. B. & Watson, E. B. 2010. Two diffusion pathways in quartz: a combined UV-laser and RBS study. *Geochimica et Cosmochimica Acta*, **74**, 5906–5925. http://dx.doi.org/10.1016/j.gca.2010.07.014

Coombs, D. S. 1954. Ferriferous orthoclase from Madagascar. *Mineralogical Magazine*, **30**, 409–427.

Dodson, M. H. 1986. Closure profiles in cooling systems. *Materials Science Forum*, **7**, 145–154.

Emmel, B., Jacobs, J., Kastowski, M. & Graser, G. 2006. Phanerozoic upper crustal tectono-thermal development of basement rocks from central Madagascar: an integrated fission-track and structural study. *Tectonophysics*, **412**, 61–86. http://dx.doi.org/10.1016/j.tecto.2005.09.008

Emmel, B., Jons, N. *et al.* 2008. From closure of the Mozambique Ocean to Gondwana breakup: new evidence from geochronological data of the Vohibory Terrain, Southwest Madagascar. *The Journal of Geology*, **116**, 21–38. http://dx.doi.org/10.1086/524121

Foland, K. A. 1974. ^{40}Ar diffusion in homogenous orthoclase and an interpretation of Ar diffusion in K-feldspars. *Geochimica et Cosmochimica Acta*, **38**, 151–166.

Grégoire, V., Nédélec, A., Monié, P., Montel, J.-M., Ganne, J. & Ralison, B. 2009. Structural reworking and heat transfer related to the late-Pan African Angavo shear zone of Madagascar. *Tectonophysics*, **477**, 197– 216. http://dx.doi.org/10.1016/j.tecto.2009.03.009

Lee, J. W. 1995. Multipath diffusion in geochronology. *Contributions to Mineralogy and Petrology*, **120**, 60–82.

London, D. 1996. Granitic pegmatites. *Geological Society of America Special Papers*, **315**, 305–319.

Lovera, O. M., Richter, F. M. & Harrison, T. M. 1989. The ^{40}Ar/^{39}Ar thermochronometry for slowly cooled samples having a distribution of diffusion domain sizes. *Journal of Geophysical Research*, **94**, 17917–17935.

Lovera, O. M., Grove, M., Harrison, T. M. & Mahon, K. I. 1997. Systematic analysis of K-feldspar ^{40}Ar/^{39}Ar step heating results: I. Significance of activation energy determinations. *Geochimica et Cosmochimica Acta*, **61**, 3171–3192. http://dx.doi.org/10.1016/S0016-7037(97)00147-6

Lovera, O. M., Grove, M. & Harrison, T. M. 2002. Systematic analysis of K-feldspar ^{40}Ar/^{39}Ar step heating results: II. Relevance of laboratory argon diffusion properties to nature. *Geochimica et Cosmochimica Acta*, **66**, 1237–1255.

Mark, D. F., Kelley, S. P., Lee, M. R., Parnell, J., Sherlock, S. C. & Brown, D. J. 2008. Ar–Ar dating of authigenic K-feldspar: quantitative modelling of radiogenic argon-loss through subgrain boundary networks. *Geochimica et Cosmochimica Acta*, **72**, 2695–2710. http://dx.doi.org/10.1016/j.gca.2008.03.018

Meert, J. G., Hall, C., Nédélec, A. & Razanatseheno, M. O. M. 2001. Cooling of a Late-Syn Orogenic Pluton: evidence from Laser K-feldspar Modelling of the Carion Granite, Madagascar. *Gondwana Research*, **4**, 541–550. http://dx.doi.org/10.1016/S1342-937X(05)70353-1

Nägler, T. F. & Villa, I. M. 2000. In pursuit of the ^{40}K branching ratios: K–Ca and ^{39}Ar–^{40}Ar dating of gem silicates. *Chemical Geology*, **169**, 5–16.

Paquette, J.-L. & Nédélec, A. 1998. A new insight into Pan-African tectonics in the East-West Gondwana collision zone by U–Pb zircon dating of granites from central Madagascar. *Earth and Planetary Science Letters*, **155**, 45–56.

Parsons, I., Rex, D. C., Guise, P. & Halliday, A. N. 1988. Argon-loss by alkali feldspars. *Geochimica et Cosmochimica Acta*, **52**, 1097–1112. http://dx.doi.org/10.1016/0016-7037(88)90264-5

Pickles, C. S., Kelley, S. P., Reddy, S. M. & Wheeler, J. 1997. Determination of high spatial resolution argon isotope variations in metamorphic biotites. *Geochimica et Cosmochimica Acta*, **61**, 3809–3833. http://dx.doi.org/10.1016/S0016-7037(97)00289-5

Reddy, S. M., Potts, G. J. & Kelley, S. P. 2001. ^{40}Ar/^{39}Ar ages in deformed potassium feldspar: evidence of microstructural control on Ar isotope systematics. *Contributions to Mineralogy and Petrology*, **141**, 186–200.

Renne, P. R., Swisher, C. C., Deino, A. L., Karner, D. B., Owens, T. L. & DePaolo, D. J. 1998. Intercalibration of standards, absolute ages and uncertainties in ^{40}Ar/^{39}Ar dating. *Chemical Geology*, **145**, 117–152. http://dx.doi.org/10.1016/S0009-2541(97)00159-9

Renne, P. R., Mundil, R., Balco, G., Min, K. & Ludwig, K. R. 2010. Joint determination of ^{40}K decay constants and ^{40}Ar*/^{40}K for the Fish Canyon sanidine standard, and improved accuracy for ^{40}Ar/^{39}Ar geochronology. *Geochimica et Cosmochimica Acta*, **74**, 5349–5376.

Renne, P. R., Mulcahy, S. R. *et al.* 2012. Retention of inherited Ar by alkali feldspar xenocrysts in a magma: kinetic constraints from Ba zoning profiles. *Geochimica et Cosmochimica Acta*, **93**, 129–142. http://dx.doi.org/10.1016/j.gca.2012.06.029

Seward, D., Grujic, D. & Schreurs, G. 2004. An insight into the breakup of Gondwana: identifying events through low-temperature thermochronology from the basement rocks of Madagascar. *Tectonics*, **23**, TC3007.

Smith, S. R., Kelley, S. P., Tindle, A. G. & Breaks, F. W. 2005. Compositional controls on ^{40}Ar/^{39}Ar ages of zoned mica from a rare-element pegmatite. *Contributions to Mineralogy and Petrology*, **149**, 613–626. http://dx.doi.org/10.1007/s00410-005-0674-7

Storey, M., Mahoney, J. J., Saunders, A. D., Duncan, R. A., Kelley, S. P. & Coffin, M. F. 1995. Timing of hot spot-related volcanism and the breakup of Madagascar and India. *Science*, **267**, 852–855. http://dx.doi.org/10.1126/science.267.5199.852

Thomas, J. B., Cherniak, D. J. & Watson, E. B. 2008. Lattice diffusion and solubility of argon in forsterite, enstatite, quartz and corundum. *Chemical Geology*, **253**, 1–22.

WARTHO, J.-A., KELLEY, S. P., BROOKER, R. A., CARROLL, M. R., VILLA, I. M. & LEE, M. R. 1999. Direct measurement of Ar diffusion profiles in a gem-quality Madagascar K-feldspar using the ultra-violet laser ablation microprobe (UVLAMP). *Earth and Planetary Science Letters*, **170**, 141–153. http://dx.doi.org/10.1016/S0012-821X(99)00088-6

WATSON, E. B. & CHERNIAK, D. J. 2003. Lattice diffusion of Ar in quartz, with constraints on Ar solubility and evidence of nanopores. *Geochimica et Cosmochimica Acta*, **67**, 2043–2062.

WHEELER, J. 1996. DIFFARG: a program for simulating argon diffusion profiles in minerals. *Computers & Geosciences*, **22**, 919–929.